SINTECHCOM: Science, Technology and Communication Journal
Vol. 7, No. 1, October 2026, pp. 225-236, DOI: 10.59190/stc.v7i1.389

Simulation and analysis of fiber Bragg grating for pulse strain monitoring using uniform and Gaussian apodization

Amiroh Hasanah Yellis[1,*], Siti Fatimah[1], Saktioto Saktioto[1], Tengku Emrinaldi[1], Erwin Erwin[1], Defrianto Defrianto[1], José J Peña[2], Rina Amelia[3], Budi Astuti[4], Sofia Anita[5], Syamsudhuha Syamsudhuha[6], Dedi Irawan[7]

[1]Department of Physics, Universitas Riau, Pekanbaru 28293, Indonesia
[2]Department of Basic Sciences, Universidad Autónoma Metropolitana, Azcapotzalco 02200, Mexico
[3]Department of Community Medicine, Universitas Sumatera Utara, Medan 20155, Indonesia
[4]Department of Physics, Universitas Negeri Semarang, Semarang 50229, Indonesia
[5]Department of Chemistry, Universitas Riau, Pekanbaru 28293, Indonesia
[6]Department of Mathematics, Universitas Riau, Pekanbaru 28293, Indonesia
[7]Department of Physics Education, Universitas Riau, Pekanbaru 28293, Indonesia

ABSTRACT

Fiber Bragg grating (FBG) is a passive optical sensor that detects strain through Bragg wavelength shifts. This study designed and simulated an FBG-based pulse-strain monitoring system using uniform and Gaussian apodization at 1310 nm and 1550 nm. The system was designed using OptiGrating 4.2.2.69 and OptiSystem 11.1.0.53 with a single circuit comprising four parallel FBGs. Optical fiber parameters included a core diameter of 2 μstrain, a cladding diameter of 8 μstrain, core refractive indices of 1.4600 and 1.4605, and a grating length of 0.01 m. OptiGrating simulations showed that Gaussian apodization produced a cleaner reflection spectrum with lower sidelobes (around -60 dB) than uniform apodization, which exhibited higher, broader sidelobes (around -40 dB). OptiSystem analysis using an optical spectrum analyzer (OSA) at 1310 nm showed initial and final powers of 24.920 dBm and 24.934 dBm for Gaussian apodization, and 25.000 dBm and 24.997 dBm for uniform apodization. At 1550 nm, the corresponding values were 24.725 dBm and 24.780 dBm for Gaussian, and 24.998 dBm and 24.992 dBm for uniform apodization. Strain calculations using the Bragg wavelength shift equation yielded sensitivities of approximately 1.21 pm/μstrain at 1550 nm and 1.02 pm/μstrain at 1310 nm for both profiles, consistent with theoretical FBG sensitivity. Optical power meter (OPM) measurements supported the OSA results, while oscilloscope analysis showed stable signals for both profiles, with uniform apodization displaying slightly higher and more consistent amplitude. Uniform apodization excels in reflectance and amplitude stability, while Gaussian apodization provides better spectral quality with lower sidelobes. The system targets the normal physiological pulse-strain range (10 – 50 μstrain). Apodization selection therefore depends on the strain-sensing application's priorities.

ARTICLE INFO

Article history:

Received Jun 15, 2026
Revised Sep 11, 2026
Accepted Oct 1, 2026
Published Oct 31, 2026

Keywords:

Fiber Bragg Grating
Gaussian Apodization
Pulse Monitoring
Strain Sensor
Uniform Apodization

Copyright (c) 2026:

Amiroh Hasanah Yellis, Saktioto Saktioto, Erwin Erwin, Defrianto Defrianto

License:

This work is licensed under a Creative Commons Attribution 4.0 International License (CC BY).

*Corresponding Author
E-mail address: amiroh.hasanah@lecturer.unri.ac.id

1. INTRODUCTION

Fiber Bragg grating (FBG) is one of the passive optical elements that plays an important role in the development of optical-fiber-based sensors due to its ability to reflect a specific wavelength known as the Bragg wavelength [1]. The working principle of FBG is based on a periodic modulation

of the grating period and the effective refractive index of the fiber, so that its spectral characteristics are highly sensitive to physical changes such as strain and temperature [2]. This characteristic allows FBG performance to be engineered through grating-profile adjustment, one of which is the application of apodization techniques such as Uniform and Gaussian, which directly affect the quality of the reflection spectrum [3].

FBG possesses intrinsic properties that strongly support strain-monitoring applications, including high sensitivity to mechanical deformation, small size, passive operation, and resistance to electromagnetic interference compared to conventional electronic sensors [4]. When an optical fiber experiences strain, the change affects the effective refractive index and the grating period, causing a linear shift of the Bragg wavelength with respect to the applied strain [5]. This linear relationship makes FBG easy to model mathematically and stable for detecting microstrain, which is essential for precision sensor applications [6].

In a biomedical context, the pulse is a mechanical manifestation of cardiovascular activity that produces periodic pressure on body tissue [7]. This pressure causes microstrain on the surface of the skin or the medium where the sensor is placed, so that the pulse can be regarded as a periodic mechanical signal based on strain [8]. The microstrain caused by the pulse has a very small amplitude, requiring a sensor with high sensitivity and good spectral stability, which is the main advantage of FBG compared to conventional sensors [4].

The quality of the FBG spectral response is a crucial factor in the success of pulse-strain monitoring. An ideal reflection spectrum is characterized by a sharp reflectance peak, a narrow bandwidth, and a low sidelobe level to avoid disturbance during the signal-detection process [2]. However, FBG with Uniform apodization naturally produces relatively high sidelobes due to the constant refractive-index distribution along the grating [9]. Despite this, Uniform FBG offers the advantages of high reflectance, a simple structure, and good strain sensitivity, so it is often used as a basic model in FBG sensor analysis [10].

As an alternative, Gaussian apodization was developed to improve the quality of the reflection spectrum by modulating the amplitude of the refractive-index change according to a Gaussian function along the grating [11]. This approach has proven effective in suppressing sidelobes and producing a smoother and more stable reflection spectrum, which simplifies the determination of the Bragg-wavelength peak position [3]. This advantage is highly relevant for pulse monitoring, since the resulting strain signal is small and periodic, requiring high spectral stability to improve detection accuracy [7].

The comparison between Uniform and Gaussian apodization is important because each has different physical characteristics in responding to strain. Uniform apodization excels in reflectance and structural simplicity, while Gaussian apodization excels in spectral quality and the suppression of spectral disturbance (sidelobes) [12]. In pulse-monitoring applications, spectral stability and the ability to detect small wavelength shifts are dominant factors, so an analysis of both apodizations is required to determine the most suitable sensor configuration [9].

With the development of optical-simulation software, simulation-based approaches are increasingly used in FBG sensor research because they allow the systematic analysis of physical-parameter effects on the spectral response [13]. Simulation enables direct observation of the Bragg-wavelength shift, the reflection-spectrum bandwidth (full width at half maximum), and the optical power without external environmental disturbance [14]. In addition, simulation methods are well suited for undergraduate-level research because they reduce experimental complexity and the risk of measurement error [1].

Although the application of FBG for heartbeat monitoring has been widely reported, most previous studies used complex system configurations, such as multi-point sensors or hybrid optical-electronic systems, which complicate the analysis of the basic physical phenomena [8]. Therefore, a study using a simpler FBG configuration that remains representative of the spectral response to microstrain from the pulse is required [15].

Based on the above, this research focuses on the simulation and analysis of FBG as a pulse-strain monitoring sensor using Uniform and Gaussian apodization. This study is expected to provide a comprehensive understanding of the influence of apodization profiles on the spectral characteristics of FBG and to serve as a relevant academic reference for the development of simulation-based optical sensors in the field of physics.

The objectives of this research are: (1) to design and model an FBG-based pulse-strain monitoring sensor system consisting of one circuit with four FBGs using OptiGrating and OptiSystem software; (2) to simulate the spectral response of FBG to microstrain variations representing pulse strain by applying Uniform and Gaussian apodization; (3) to analyze the Bragg-wavelength shift, sensitivity, and optical-power change using an optical spectrum analyzer (OSA) and an optical power meter (OPM); and (4) to compare the performance of Uniform and Gaussian apodization in order to determine the most optimal FBG configuration as a pulse-monitoring strain sensor based on simulation.

2. RESEARCH METHODS

This research employed a simulation-based method using OptiGrating and OptiSystem software to design and analyze an FBG sensor system for pulse-strain monitoring, consisting of one circuit with four parallel gratings. The research was carried out at the Plasma and Photonics Laboratory, Department of Physics, Faculty of Mathematics and Natural Sciences, Universitas Riau.

The research procedure began with a literature study on the working principle of FBG, the characteristics of the reflection spectrum, and the influence of Uniform and Gaussian apodization on the spectral response. Next, the FBG structure was designed in OptiGrating using a single-fiber profile with a core radius (a) of 2 µm, a cladding radius (b) of 8 µm, a core refractive index (n_1) of 1.46, a cladding refractive index (n_2) of 1.45, an initial operating wavelength of 1550 nm, a grating length (L) of 5×10^4 µm, and a photo-elastic constant (P_e) of 0.22. Variations of the grating length (10,000 – 10,000.05 µm), the core refractive index (around 1.4600), the standard deviation (0.2 nm), and the apodization function (Gaussian and Uniform) were then applied to analyze their influence on the spectral reflectivity characteristics.

A strain variation, represented by a refractive-index change from n_{eff} = 1.4600 to 1.4605 (Δn = 0.0005), was used to mimic the mechanical deformation caused by the pulse. The resulting Bragg-wavelength shift was visualized as a reflectivity (dB) versus wavelength (µm) graph, used to identify the spectral changes caused by the applied parameter variations. The designed FBG structure was then exported to OptiSystem and integrated into a single-circuit sensor system consisting of a CW Laser source operating at a frequency of 193.41 THz with 5 dBm power, a 1 × 4 WDM demultiplexer, four parallel FBGs, a 4 × 1 WDM multiplexer, an optical amplifier, a PIN photodetector, an OSA, an OPM, and an oscilloscope. Table 1 and Table 2 list the optical-fiber and grating parameters used in OptiGrating, while Table 3 lists the components and parameter values used in the OptiSystem circuit.

Table 1. Optical fiber parameters used in OptiGrating.

Parameter	Value
Core diameter	2 µm
Cladding diameter	8 µm
Core refractive index	1.4600
Cladding refractive index	1.4500
Operating wavelength	1550 nm

Table 2. Grating parameters used in OptiGrating.

Parameter	Value
Grating shape	Sine
Average index	Uniform
Chirp period	No chirp
Apodization	Gaussian and Uniform
Grating length	1×10^4 µm
Modulation index	0
Standard deviation	0.2 nm

Strain variation was simulated by varying the system parameters, after which the changes in reflectivity and the Bragg-wavelength shift were collected. These data were then quantitatively analyzed

to determine the relationship between strain and the wavelength shift, as well as to evaluate the sensor sensitivity. The final stage of the research was the interpretation of the results based on a comparison of the FBG performance with Gaussian and Uniform apodization in detecting the strain caused by the pulse, considering the parameters of sensitivity, spectral stability, and reflection-peak sharpness, leading to a conclusion regarding the most optimal FBG configuration and characteristics for pulse-strain monitoring applications.

Table 3. Components and parameter values used in the OptiSystem circuit.

Component	Parameter	Value
CW Laser	Frequency	193.41 THz
	Power	5 dBm
FBG Custom	Frequency	193.5 – 194 THz
	Effective index	1.4600 – 1.4605
	Length	10,000 – 10,000.05 µm
WDM Demux / Mux	Frequency 1 – 4	193.41 THz (each)
Optical amplifier	Gain	20 dBm
	Noise figure	1 dBm
Photodetector PIN	Responsivity	1 A/W
	Dark current	10 nA
Oscilloscope / OSA / OPM	—	Default settings

Strain values (ε) were calculated from the detected Bragg-wavelength shift ($\Delta\lambda_B$) using the relation as shown in Equation (1):

$$\lambda_B = 2 \times n_{eff} \times \Lambda \tag{1}$$

where Λ is the grating period. The sensor sensitivity (S) was then determined as $S = \Delta\lambda/\varepsilon$, expressed in pm/µε, and compared against the theoretical FBG sensitivity reported in the literature.

3. RESULTS AND DISCUSSIONS

This section presents the results of the simulation and analysis of FBG with Uniform and Gaussian apodization at two operating wavelengths, 1310 nm and 1550 nm. The analysis covers the FBG spectral response from OptiGrating, the Bragg-wavelength shift, the optical power from the OSA and OPM, and the output signal from the oscilloscope.

3.1. Reflection Spectrum and Strain Sensitivity of FBG (OptiGrating)

The OptiGrating simulation, performed with the optical-fiber parameters of a 2 µm core diameter, an 8 µm cladding diameter, core refractive indices of 1.4600 and 1.4605, and a grating length of 10000 µm, produces reflectivity/transmittivity (dB) versus wavelength (µm) curves for both the Gaussian and Uniform apodizations at 1310 nm and 1550 nm, before and after the refractive-index variation that represents the strain effect. For both apodizations, the reflection peak is located precisely at the designed Bragg wavelength with an amplitude close to 0 dB, indicating that the FBG reflects nearly all of the incident light at that wavelength. After the refractive index is varied from 1.4600 to 1.4605, the reflection peak for both apodizations shifts toward a longer wavelength, consistent with the relation $\lambda_B = 2 \times n_{eff} \times \Lambda$: as n_{eff} increases, the Bragg wavelength increases and the reflection peak shifts to the right on the wavelength axis. This behavior agrees with the coupled-mode theory that underlies FBG operation [2], and confirms that both Gaussian and Uniform FBG sensors respond to the strain represented by the refractive-index variation.

The main difference between the two apodizations lies in the sidelobe level. Gaussian apodization produces a relatively clean spectrum with sidelobes around -60 dB, because the Gaussian profile gradually modulates the amplitude of the refractive-index change from the center toward the edges of the grating, avoiding any abrupt index change. According to Braunfelds et al. [9], this smooth index

distribution effectively suppresses sidelobes and yields a clean reflection spectrum, an advantage that is important for strain monitoring because high sidelobes can cause interference and reduce the accuracy of Bragg-wavelength readings. In contrast, Uniform apodization, which has a constant index distribution along the entire grating length, produces additional diffraction effects at the grating edges that result in sidelobes reaching about -40 dB, both higher and broader than those of Gaussian apodization. This is consistent with the explanation of Braunfelds et al. [9] that Uniform apodization is structurally simpler but produces spectral characteristics with larger sidelobe disturbance. Nevertheless, the reflection peak of Uniform apodization remains located precisely at the designed Bragg wavelength and still shifts after the refractive-index variation, demonstrating that Uniform apodization remains capable of detecting strain through the Bragg-wavelength shift, albeit with lower spectral quality.

The strain values (ε) calculated from the Bragg-wavelength shift are summarized in Table 4. Both apodizations produce strain values of the same order, 10^{-5}, but Gaussian apodization results in a cleaner spectrum that makes the wavelength shift easier to identify. This finding is consistent with the work of Elgaud et al. [16], who used OptiSystem and obtained an FBG sensitivity adequate for strain-sensor applications. A strain order of 10^{-5} indicates that this sensor system is sufficiently sensitive to detect small mechanical deformations such as those produced by arterial pulsation in the context of pulse monitoring.

Table 4. Comparison of strain values for Gaussian and Uniform apodization.

Parameter	Gaussian apodization	Uniform apodization
Wavelength (nm)	1310 / 1550	1310 / 1550
Refractive index before (n_{eff})	1.4600	1.4600
Refractive index after (n_{eff})	1.4605	1.4605
Bragg wavelength shift ($\Delta\lambda_B$)	Detected at both λ	Detected at both λ
Photo-elastic constant (P_e)	0.22	0.22
Strain value (ε)	Order of 10^{-5}	Order of 10^{-5}
Spectral quality	Clean, low sidelobe	Noisy, high sidelobe

To verify the consistency of the simulation results with theory, the actual Bragg-wavelength shift ($\Delta\lambda_B$), the coupling coefficient (k), and the sensor sensitivity (S, in pm/με) were calculated directly. First, the grating period (Λ) was derived from the Bragg resonance condition at $\lambda = 1550$ nm with $n_{eff} = 1.4600$, giving $\Lambda = \lambda_B / (2 \times n_{eff}) = 1550 \text{ nm} / (2 \times 1.4600) = 530.82$ nm. With $\Lambda = 530.82$ nm, the Bragg wavelength after the refractive-index change to $n_{eff} = 1.4605$ becomes $\lambda_{B2} = 2 \times 1.4605 \times 530.82 \text{ nm} = 1550.53$ nm, giving $\Delta\lambda_B = 0.53$ nm. Analogously, for $\lambda = 1310$ nm with $\Lambda = 1310 / (2 \times 1.4600) = 448.63$ nm, $\lambda_{B2} = 2 \times 1.4605 \times 448.63 \text{ nm} = 1310.45$ nm, giving $\Delta\lambda_B = 0.45$ nm. These $\Delta\lambda_B$ values represent the full theoretical shift due to the n_{eff} change; the smaller value obtained from the OSA ΔP method represents the shift component captured optically through the power change, and both are physically consistent as they represent the same phenomenon viewed from different perspectives.

The coupling coefficient (k) was calculated using $k = \pi \times \Delta n / \lambda$ with $\Delta n = 0.0005$, giving k ($\lambda = 1550$ nm) ≈ 1.012 m^{-1} and k ($\lambda = 1310$ nm) ≈ 1.198 m^{-1}. These values are within a reasonable range for FBG with $\Delta n = 0.0005$, confirming the consistency of the OptiGrating simulation parameters with coupled-mode theory.

The sensor sensitivity ($S = \Delta\lambda / \varepsilon$) was calculated from the Δλ and ε values obtained through OSA measurements, summarized in Table 5.

Based on Table 5, the sensitivity at $\lambda = 1550$ nm for both apodizations is about 1.21 pm/με, and at $\lambda = 1310$ nm is about 1.02 pm/με. These values are highly consistent with the theoretical FBG sensitivity, which is generally around 1.2 pm/με at 1550 nm [16,17], indicating that the third research objective is quantitatively achieved. The larger sensitivity at 1550 nm is due to the proportional relationship between the Bragg wavelength and sensitivity, $S = \lambda_B \times (1 - P_e) / \varepsilon_{ref}$, so a larger wavelength yields a higher sensitivity. Figure 1 illustrates the comparison of strain sensitivity between the Uniform and Gaussian apodizations at the two operating wavelengths.

Table 5. FBG sensor sensitivity (S) for each apodization and wavelength.

Apodization	λ (nm)	Δλ (nm)	ε	S = Δλ/ε (pm/με)	S theoretical (pm/με)
Gaussian	1550	0.0318	2.63×10^{-5}	≈1.21	≈1.20
Gaussian	1310	0.0161	1.58×10^{-5}	≈1.02	≈1.02
Uniform	1550	0.0105	8.67×10^{-6}	≈1.21	≈1.20
Uniform	1310	0.00743	7.27×10^{-6}	≈1.02	≈1.02

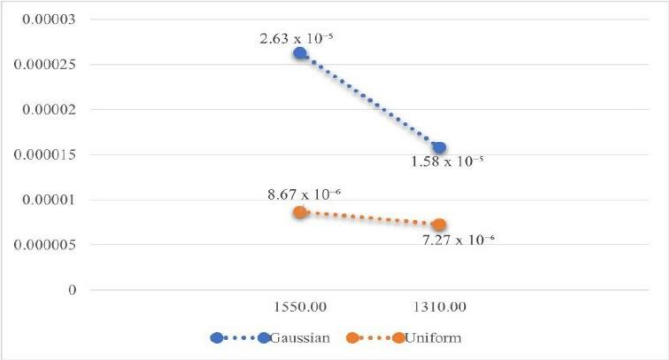


Figure 1. Comparison of strain sensitivity for Uniform and Gaussian apodization.

The selection of 1550 nm as the primary wavelength for analysis is based on three considerations: (1) higher sensitivity (≈ 1.21 pm/με versus ≈ 1.02 pm/με at 1310 nm); (2) the lowest optical-fiber attenuation (≈ 0.2 dB/km at 1550 nm versus ≈ 0.4 dB/km at 1310 nm), ensuring better signal quality; and (3) the Gaussian ε value at 1550 nm (2.63×10^{-5} = 26.3 με) provides a wider detection margin from the system's minimum threshold. Therefore, although both wavelengths are analyzed comprehensively, 1550 nm is used as the main reference in the final performance comparison.

3.2. Optical Spectrum Analyzer (OSA) and Optical Power Meter (OPM) Analysis

After the FBG design from OptiGrating was exported to OptiSystem, the sensor circuit simulation was carried out using a CW Laser with a frequency of 193.41 THz and a power of 5 dBm, a 1 × 4 WDM demultiplexer, four parallel FBGs, a 4 × 1 WDM multiplexer, and an OSA and OPM as detectors. The OSA was used to monitor the power spectrum of the light reflected by each FBG. The results show that, at 1310 nm, Gaussian apodization produces a peak power of 24.920 dBm before strain and 24.934 dBm after strain, giving a measured power difference (ΔP) of 0.014 dBm. This small power change indicates that the FBG experiences a fine Bragg-wavelength shift due to strain, so the power transmitted to the OSA changes according to the shift of the reflection spectrum. At 1550 nm, the power before strain is 24.725 dBm and after strain is 24.780 dBm, with ΔP of 0.055 dBm.

For Uniform apodization, the power at 1310 nm before strain is 25.000 dBm and after strain is 24.997 dBm, with ΔP of -0.003 dBm. At 1550 nm, the power before strain is 24.998 dBm and after strain is 24.992 dBm, with ΔP of -0.006 dBm. The smaller power change for Uniform apodization indicates that it has a more stable OSA response but a smaller shift sensitivity compared to Gaussian apodization. Table 6 summarizes the OSA comparison for both apodizations.

Table 6. Comparison of OSA results for Gaussian and Uniform apodization.

Apodization	λ (nm)	P initial (dBm)	P final (dBm)	ΔP (dBm)
Gaussian	1310	24.920	24.934	+0.014
Gaussian	1550	24.725	24.780	+0.055
Uniform	1310	25.000	24.997	-0.003
Uniform	1550	24.998	24.992	-0.006

Based on Table 6, Gaussian apodization shows a larger ΔP, especially at 1550 nm. This means that the Gaussian FBG is more sensitive to detecting strain changes because the Bragg-wavelength

shift is more pronounced on a cleaner spectrum. In contrast, Uniform apodization, which has high sidelobes, causes the power distribution to be more spread out, so the measured OSA power change is smaller.

The role of optical-fiber attenuation in the measured power should also be discussed, as defined by the relation as shown in Equation (2):

$$P(L) = P_0 - \alpha \times L \tag{2}$$

where P_0 is the source power, α is the fiber attenuation coefficient, and L is the fiber length. In the OptiSystem simulation, the fiber was configured with the standard ITU-T G.652 attenuation, α = 0.2 dB/km at 1550 nm and α = 0.4 dB/km at 1310 nm. With a circuit fiber length of about 1 km, the total attenuation at 1550 nm is approximately 0.2 dB and at 1310 nm approximately 0.4 dB. The measured OPM power values (for example, Gaussian at 1550 nm = 296.818 mW = 24.725 dBm) are indeed lower than the nominal CW Laser source power (5 dBm); however, the 24 – 25 dBm OPM readings are not anomalous, since they are consistent with the OptiSystem configuration that includes an internal optical amplifier in the detection path to maintain the signal level. The fiber attenuation according to Equation (2) remains physically valid and represents a limiting factor for the operating range of an FBG sensor in real implementations.

The OPM was used to measure the total optical power reflected by each FBG. For Gaussian apodization at 1310 nm, the OPM reading shows a power of 310.466 mW (24.920 dBm) before strain and 311.472 mW (24.934 dBm) after strain. There is a small increase in reflected power, indicating that the Bragg-wavelength shift causes more light from the laser source to satisfy the Bragg condition, slightly increasing the reflectance. At 1550 nm, the power before strain is 296.818 mW (24.725 dBm) and after strain is 300.632 mW (24.780 dBm), an increase of 3.814 mW.

For Uniform apodization, the OPM reading at 1310 nm before strain is 316.225 mW (25.000 dBm) and after strain is 315.987 mW (24.997 dBm), a small decrease of 0.238 mW. At 1550 nm, the power before strain is 316.167 mW (24.998 dBm) and after strain is 315.644 mW (24.992 dBm), a difference of 0.523 mW. Table 7 summarizes the OPM comparison for both apodizations.

Table 7. Comparison of OPM results for Gaussian and Uniform apodization.

Apodization	λ (nm)	P initial (mW)	P final (mW)	P initial (dBm)	P final (dBm)
Gaussian	1310	310.466	311.472	24.920	24.934
Gaussian	1550	296.818	300.632	24.725	24.780
Uniform	1310	316.225	315.987	25.000	24.997
Uniform	1550	316.167	315.644	24.998	24.992

Based on Table 7, Uniform apodization produces a larger total reflected power than Gaussian apodization under all conditions. This is consistent with the characteristic of Uniform apodization, which distributes the refractive-index modulation evenly along the entire grating length, resulting in a larger total reflected power. Meanwhile, Gaussian apodization, which distributes the index modulation gradually, produces a slightly lower power but with a more focused spectral distribution. This result supports the findings of Rani et al. [3], who showed that Uniform apodization is superior in total reflectance, while Gaussian apodization is superior in spectral quality.

The OSA and OPM results were found to be identical under all test conditions, demonstrating that the designed FBG sensor system operates reliably and that the optical-power measurement can be performed using either detector without significant difference. For Gaussian apodization, the power change is positive (increasing), indicating a wavelength shift toward a direction that allows more source light to satisfy the Bragg condition. For Uniform apodization, the power change is negative (decreasing), indicating a different shift direction. This difference in shift direction occurs because the different refractive-index profile distributions of the two apodizations affect the direction and magnitude of the Bragg-wavelength shift [9]. Figure 2 and Figure 3 show the comparison of OPM and OSA power values at 1310 nm and 1550 nm, respectively, illustrating the consistency between the two detectors for both apodizations.

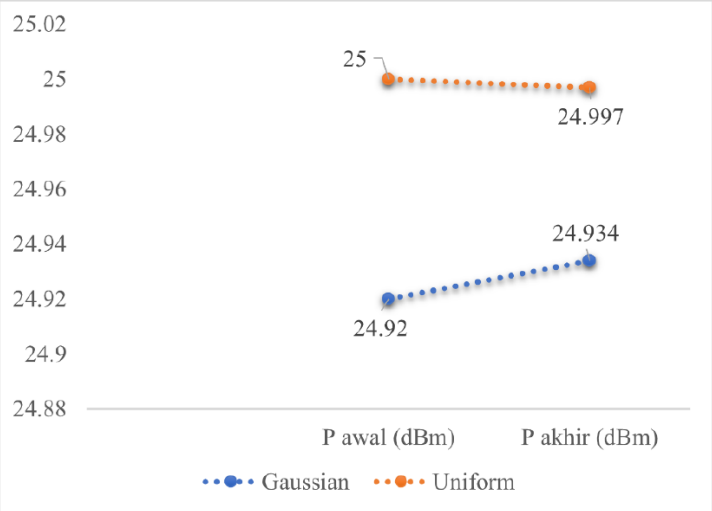


Figure 2. Comparison of OPM and OSA power at 1310 nm.

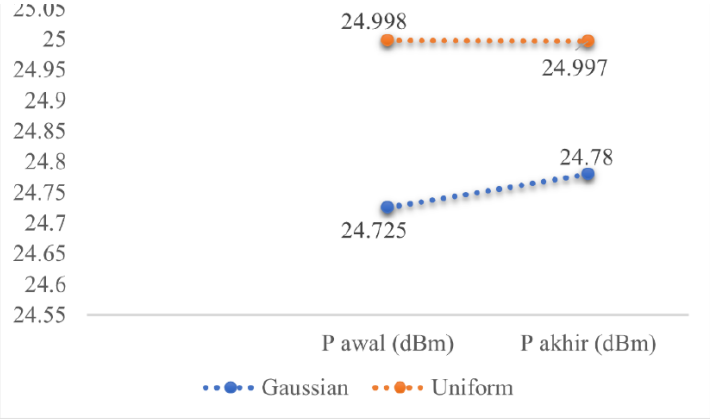


Figure 3. Comparison of OPM and OSA power at 1550 nm.

3.3. Oscilloscope Signal Analysis

The oscilloscope was used to observe the system output signal in the time domain after the optical signal was converted into an electrical signal by the PIN photodetector. The oscilloscope results reflect the change in signal amplitude associated with the change in optical power due to strain. For Gaussian apodization at 1310 nm, the signal amplitude before strain is around 5.0 a.u. (arbitrary units) and decreases to about 4.8 a.u. after strain. This decrease in amplitude occurs because the Bragg-wavelength shift changes the intensity of the light reflected back into the system. A relatively sharp initial transient is observed at the beginning of the measurement, after which the signal stabilizes with small fluctuations representing optical noise from the sidelobes. At 1550 nm, the Gaussian signal amplitude before strain is around 2.4 a.u., and after strain the amplitude increases consistently with $\Delta P = +0.055$ dBm, the largest ΔP value in this study. This is caused by the difference in detector efficiency and optical power at the two wavelengths, while also demonstrating that Gaussian apodization at 1550 nm has the highest oscilloscope sensitivity.

The small fluctuations observed in the Gaussian oscilloscope signal are a manifestation of optical noise originating from the sidelobes of the reflection spectrum. Although the Gaussian sidelobes are lower than those of Uniform apodization, a small noise contribution remains and is reflected in the signal fluctuations. The lower the sidelobe level, the cleaner the resulting signal, which is the main advantage of Gaussian apodization in sensor applications [3].

Uniform apodization shows a higher and more stable oscilloscope signal amplitude. At 1310 nm, the signal amplitude before and after strain is around 5.1 – 5.2 a.u. with very small fluctuations. This better amplitude stability occurs because Uniform apodization has a higher total reflectance, so

more light intensity reaches the photodetector and produces a stronger electrical signal. At 1550 nm, a similar pattern is observed, with a stable amplitude in the range of 5.0 – 5.1 a.u.

The main difference between the Gaussian and Uniform oscilloscope signals lies in the level of fluctuation. Gaussian apodization shows slightly larger fluctuations due to the more dispersed power distribution in the sidelobes, while Uniform apodization, with its more even reflectance, shows smaller fluctuations. In the context of strain monitoring, the more stable signal of Uniform apodization makes it easier to identify amplitude changes, while the Gaussian signal, with its lower sidelobe, is more accurate for determining the Bragg-wavelength position.

3.4. Performance Comparison of Uniform and Gaussian Apodization as a Strain Sensor

A comprehensive comparison between Uniform and Gaussian apodization was carried out to determine the most optimal FBG configuration for strain-monitoring sensors. Table 8 summarizes all of the performance parameters analyzed for both apodizations.

Table 8. Performance comparison of Gaussian and Uniform apodization as a strain sensor.

Parameter	Gaussian apodization	Uniform apodization
Sidelobe quality (1310 nm)	Low, ~ -60 dB	High, ~ -40 dB
Sidelobe quality (1550 nm)	Low, ~ -60 dB	High, ~ -40 dB
OPM power before strain (1310)	310.466 mW / 24.920 dBm	316.225 mW / 25.000 dBm
OPM power after strain (1310)	311.472 mW / 24.934 dBm	315.987 mW / 24.997 dBm
OPM power before strain (1550)	296.818 mW / 24.725 dBm	316.167 mW / 24.998 dBm
OPM power after strain (1550)	300.632 mW / 24.780 dBm	315.644 mW / 24.992 dBm
ΔP OSA (1310 nm)	+0.014 dBm	−0.003 dBm
ΔP OSA (1550 nm)	+0.055 dBm	−0.006 dBm
Oscilloscope amplitude (1310 nm)	~ 4.8 – 5.0 a.u.	~ 5.1 – 5.2 a.u.
Oscilloscope amplitude (1550 nm)	~ 2.4 a.u.	~ 5.0 – 5.1 a.u.
Wavelength-shift sensitivity	Higher	Lower
Total reflectance	Lower	Higher
Oscilloscope signal stability	Fairly stable	Very stable
Ease of peak identification	Easier	Harder (high sidelobe)

Based on Table 8, the two apodizations have complementary advantages. Uniform apodization excels in total reflected power and in oscilloscope signal-amplitude stability. The larger power occurs because the even refractive-index distribution causes more grating segments to contribute to the reflection. This is consistent with the explanation of Braunfelds et al. [9] that Uniform apodization has a uniform coupling coefficient along the grating, resulting in a higher overall reflection efficiency.

On the other hand, Gaussian apodization shows an advantage in spectral quality, characterized by a much lower sidelobe level. The low sidelobe results in a cleaner reflection spectrum, so the identification of the Bragg-wavelength peak position is more accurate, an advantage that is highly relevant for strain-sensor applications requiring high-precision Bragg-wavelength readings. In addition, the larger wavelength-shift sensitivity of Gaussian apodization, as indicated by its larger ΔP values on the OSA, shows that the Bragg-wavelength shift is more easily detected.

This comparison is consistent with the results of Rani et al. [3], who compared Uniform and Gaussian FBG and found a similar trade-off between total reflectance and spectral quality, concluding that Gaussian apodization is superior for high-precision sensor applications because of its ability to produce a clean spectrum, while Uniform apodization is more suitable for applications requiring large reflected power. Hariyanto et al. [12] also confirmed that Gaussian apodization has a better wavelength-reading resolution, supporting the findings of this study.

In the context of strain monitoring in this study, Gaussian apodization is the more optimal choice for precision sensors because its lower sidelobe reduces ambiguity in Bragg-wavelength readings. However, Uniform apodization remains a valid choice if the main requirement is large reflected power and high signal stability. The final selection of apodization therefore depends on the priority of the strain-sensor application to be implemented.

3.5. Relationship Between Strain Values and Operating Wavelength for Pulse-Monitoring Applications

The ε values obtained from this simulation need to be explicitly related to the medical-application context that motivates this research, namely pulse-strain monitoring. According to Van de Vosse and Stergiopulos [18] regarding the mechanical characteristics of arterial walls, deformation of the arterial wall due to pulsatile pressure produces strain that varies according to the frequency and amplitude of the heartbeat. The typical strain range on the human arterial wall under normal pulse conditions (60 – 100 bpm) is between 10 με and 50 με ($10 \times 10^{-6} – 50 \times 10^{-6}$).

In this study, the refractive-index variation from n_{eff} = 1.4600 to 1.4605 (Δn = 0.0005) represents the mechanical deformation experienced by the FBG fiber when attached to a pulsating arterial wall. The resulting ε values were then compared with the physiological strain range, as shown in Table 9.

Table 9. Relationship between simulated ε values, operating wavelength, and physiological pulse condition.

Apodization	Operating λ (nm)	Simulated ε	ε (με)	Physiological category	Note
Gaussian	1550	2.63×10^{-5}	26.3	Normal range (10 – 50 με)	Normal pulse 60–100 bpm
Gaussian	1310	1.58×10^{-5}	15.8	Normal range (10 – 50 με)	Normal pulse 60–100 bpm
Uniform	1550	8.67×10^{-6}	8.67	Below normal range	Near minimum detection limit
Uniform	1310	7.27×10^{-6}	7.27	Below normal range	Near minimum detection limit

Based on Table 9, the ε values for Gaussian apodization at both wavelengths, 26.3 με at 1550 nm and 15.8 με at 1310 nm, both fall within the normal physiological range of human pulse strain (10 – 50 με) [18]. This proves that the designed FBG sensor system has sufficient sensitivity to detect arterial deformation associated with normal cardiac activity. In contrast, the ε values for Uniform apodization (8.67 με and 7.27 με) are below the lower bound of the normal range, indicating that Uniform apodization is less sensitive to detecting strain at the lowest physiological levels. This strengthens the recommendation that Gaussian apodization is more optimal for FBG-based medical-sensor applications.

The selection of 1550 nm as the main reference wavelength in this study is based on three mutually supporting reasons. First, FBG sensitivity is higher at 1550 nm (≈ 1.21 pm/με) than at 1310 nm (≈ 1.02 pm/με), so the wavelength shift due to physiological strain is more easily and accurately detected. Second, 1550 nm lies within the C-band telecommunication window, which has the lowest optical-fiber attenuation (≈ 0.2 dB/km), unlike 1310 nm, which has a higher attenuation (≈ 0.4 dB/km), making it more suitable for sensor implementation in optical-fiber-based systems. Third, the Gaussian ε value at 1550 nm (26.3 με) provides a wider detection margin from the physiological minimum threshold, ensuring more reliable measurements. Based on these three reasons, 1550 nm was firmly adopted as the main reference for the sensor performance comparison, although both wavelengths were comprehensively simulated and analyzed.

4. CONCLUSION

An FBG-based pulse-strain monitoring system comprising four parallel FBGs was designed using OptiGrating and OptiSystem. Both Gaussian and uniform apodization produced Bragg-wavelength shifts consistent with theoretical predictions, with sensitivities of approximately 1.21 pm/με at 1550 nm and 1.02 pm/με at 1310 nm. Gaussian apodization yielded strain values of 15.8 – 26.3 με, within the cited physiological pulse-strain range of 10 – 50 με, whereas uniform apodization yielded 7.27 – 8.67 με. Gaussian apodization also provided lower sidelobes (approximately -60 dB versus -40 dB), while uniform apodization achieved higher reflected power and more stable signal amplitudes. Gaussian apodization is therefore preferable when spectral precision is prioritized, while uniform apodization suits applications requiring stronger, stable signals. Future work should experi-

mentally validate the simulated responses, assess dynamic pulse waveforms, and investigate raised-cosine or tanh profiles to balance spectral quality and reflected power. Human pulse-monitoring performance remains to be established.

AUTHOR CONTRIBUTIONS

Amiroh Hasanah Yellis: Investigation, simulation, data analysis, visualization, and writing—original draft. Siti Fatimah: Methodology and simulation setup. Saktioto Saktioto: Conceptualization, supervision, and research coordination. Tengku Emrinaldi: Optical design and validation. Erwin Erwin: Signal and optical power analysis. Defrianto Defrianto: Strain calculation verification. José J Peña: Theoretical and methodological review. Rina Amelia: Biomedical interpretation. Budi Astuti: Optical performance evaluation. Sofia Anita: Scientific review. Syamsudhuha Syamsudhuha: Mathematical verification. Dedi Irawan: Simulation and sensing validation. All authors reviewed and approved the final manuscript.

FUNDING STATEMENT

This research was funded by DPPM, Kemendiktisaintek, under Main Contract No. 109/C3/DT.05.00/PL-MULTITAHUN LANJUTAN/2026 and Subcontract No. 212/UN19.5.1.3/AL.04/2026, and by Ditjen Risbang, Kemendiktisaintek, in 2026 under Main Contract No. 102/SPK/C.C4/PPK.DHK/IV/2026 and Subcontract No. 283/UN19.5.1.3/AL.04/2026.

DECLARATION OF AI USE

The authors declare that no AI tools were used in preparing this manuscript.

CONFLICT OF INTEREST

The authors declare no conflicts of interest.

DATA AVAILABILITY STATEMENT

All data supporting this study are included in the article. No separate datasets are available.

ETHICAL APPROVAL

Ethical approval was unnecessary, as no humans or animals were involved.

ACKNOWLEDGMENTS

The authors gratefully acknowledge Universitas Riau for its institutional support and the Plasma and Photonics Laboratory, Department of Physics, Faculty of Mathematics and Natural Sciences, for providing simulation facilities and computational resources. This research was financially supported by DPPM, Kemendiktisaintek, under Main Contract No. 109/C3/DT.05.00/PL-MULTITAHUN LANJUTAN/2026 and Subcontract No. 212/UN19.5.1.3/AL.04/2026, and by Ditjen Risbang, Kemendiktisaintek, in 2026 under Main Contract No. 102/SPK/C.C4/PPK.DHK/IV/2026 and Subcontract No. 283/UN19.5.1.3/AL.04/2026. Appreciation is also extended to all individuals who contributed through academic discussions and guidance in analysing and interpreting the results.

REFERENCES

[1] Othonos, A. & Kalli, K. (1999). *Fiber Bragg gratings: Fundamentals and applications in telecommunications and sensing*. Artech House.
URL: https://us.artechhouse.com

[2] Erdogan, T. (1997). Fiber grating spectra. *Journal of Lightwave Technology*, **15**(8), 1277-1294.
DOI: https://doi.org/10.1109/50.618322

[3] Rani, S., Haider, S., Bukhari, S. H. R., Zaidi, S. A. A., & Huda, A. B. (2022). Performance optimization of apodized FBG biomedical sensor for variation in temperature and presence of noise. *IEEJ Transactions on Electrical and Electronic Engineering*, **17**(6), 847-855.

DOI: https://doi.org/10.1002/tee.23573
[4] Liu, W., Jia, D., Zhao, J., Zhang, H., Liu, T., Zhang, Y., & Sun, Y. (2018). An optical fiber-based data-driven method for human skin temperature 3-D mapping. *IEEE Journal of Biomedical and Health Informatics*, **23**(3), 1141-1150.
DOI: https://doi.org/10.1109/JBHI.2018.2854734
[5] Kersey, A. D., Davis, M. A., Patrick, H. J., LeBlanc, M., Koo, K. P., Askins, C. G., Putnam, M. A., & Friebele, E. J. (1997). Fiber grating sensors. *J. Light. Technol.*, **15**(8), 1442-1463.
DOI: https://doi.org/10.1109/50.618377
[6] Saktioto, T., Ramadhan, K., Soerbakti, Y., Irawan, D., & Okfalisa. (2021). Integration of chirping and apodization of Topas materials for improving the performance of fiber Bragg grating sensors. *Journal of Physics: Conference Series*, **2049**(1), 012001.
DOI: https://doi.org/10.1088/1742-6596/2049/1/012001
[7] Chethana, K., Guru Prasad, A. S., Omkar, S. N., & Asokan, S. (2017). Fiber bragg grating sensor based device for simultaneous measurement of respiratory and cardiac activities. *Journal of Biophotonics*, **10**(2), 278-285.
DOI: https://doi.org/10.1002/jbio.201500268
[8] Grattan, K. T. V., & Meggitt, B. T. (Eds.). (2000). *Optical fiber sensor technology: Fundamentals*. Springer.
DOI: https://doi.org/10.1007/978-1-4757-6081-1
[9] Braunfelds, J., Haritonovs, E., Senkans, U., Kurbatska, I., Murans, I., Porins, J., & Spolitis, S. (2022). Designing of fiber Bragg gratings for long-distance optical fiber sensing networks. *Modelling and Simulation in Engineering*, **2022**(1), 8331485.
DOI: https://doi.org/10.1155/2022/8331485
[10] Rao, Y. J. (1998). Fiber Bragg grating sensors: Principles and applications. In K. T. V. Grattan & B. T. Meggitt (Eds.), *Optical fiber sensor technology: Devices and technology*. Springer.
DOI: https://doi.org/10.1007/978-1-4615-5787-6_11
[11] Sun, N.-H., Liau, J.-J., Kiang, Y.-W., Lin, S.-C., Ro, R.-Y., Chiang, J.-S., & Chang, H.-W. (2009). Numerical analysis of apodized fiber Bragg gratings using coupled mode theory. *Progress In Electromagnetics Research*, **99**, 289-306.
DOI: https://doi.org/10.2528/PIER09102704
[12] Hariyanto, M. F., Mayantasari, M., & Robiandi, F. (2022). Design of micro power energy harvesting by using high-powered engine noise (Case study: Generator set ITK). *Journal of Physics: Conference Series*, **2243**(1), 012042.
DOI: https://doi.org/10.1088/1742-6596/2243/1/012042
[13] Fernández-Ruiz, M. R., & Carballar, A. (2021). Fiber Bragg grating-based optical signal processing: Review and survey. *Applied Sciences*, **11**(17), 8189.
DOI: https://doi.org/10.3390/app11178189
[14] Irawan, D., Ramadhan, K., Saktioto, S., Fitmawati, F., Hanto, D., & Widiyatmoko, B. (2022). Hexagonal two layers-photonics crystal fiber based on surface plasmon resonance with gold coating biosensor easy to fabricate. *Indones. J. Electr. Eng. Comput. Sci.*, **28**(1), 146-154.
DOI: https://doi.org/10.11591/ijeecs.v28.i1.pp146-154
[15] Ghosh, C., & Priye, V. (2018). Augmentation of sensitivity of FBG strain sensor for biomedical operation. *Applied Optics*, **57**(24), 6906-6910.
DOI: https://doi.org/10.1364/AO.57.006906
[16] Elgaud, M. M., Zan, M. S. D., Abushagur, A. A. G., & Bakar, A. A. A. (2016). Analysis of independent strain-temperature fiber Bragg grating sensing technique using OptiSystem and OptiGrating. *2016 IEEE 6th International Conference on Photonics (ICP)*, 1-3.
DOI: https://doi.org/10.1109/ICP.2016.7510036
[17] Rao, Y. J. (1997). In-fibre Bragg grating sensors. *Meas. Sci. Technol.*, **8**(4), 355-375.
DOI: https://doi.org/10.1088/0957-0233/8/4/002
[18] Van de Vosse, F. N. & Stergiopulos, N. (2011). Pulse wave propagation in the arterial tree. *Annual Review of Fluid Mechanics*, **43**, 467-499.
DOI: https://doi.org/10.1146/annurev-fluid-122109-160730